The Intravascular Contribution to fMRI Signal Change: Monte Carlo Modeling and Diffusion-Weighted Studies *in Vivo*

Jerrold L. Boxerman, Peter A. Bandettini, Kenneth K. Kwong, John R. Baker, Timothy L. Davis, Bruce R. Rosen, Robert M. Weisskoff

Understanding the relationship between fMRI signal changes and activated cortex is paramount to successful mapping of neuronal activity. To this end, the relative extravascular and intravascular contribution to fMRI signal change from capillaries (localized), venules (less localized) and macrovessels (remote, draining veins) must be determined. In this work, the authors assessed both the extravascular and intravascular contribution to blood oxygenation level-dependent gradient echo signal change at 1.5 T by using a Monte Carlo model for susceptibility-based contrast in conjunction with a physiological model for neuronal activation-induced changes in oxygenation and vascular volume fraction. The authors compared our Model results with experimental fMRI signal changes with and without velocity sensitization via bipolar gradients to null the intravascular signal. The model and experimental results are in agreement and suggest that the intravascular spins account for the majority of fMRI signal change on T_2*-weighted images at 1.5 T.

Key words: diffusion-weighted functional MRI; Monte Carlo modeling; susceptibility contrast; intravascular BOLD contrast.

INTRODUCTION

Several biophysical models for blood oxygenation level-dependent (BOLD) fMRI signal changes associated with task activation-induced cerebral neuronal activity have been described previously (1–3). Compartmentalization of deoxyhemoglobin establishes a magnetic susceptibility difference between the intravascular (IV) and extravascular (EV) space that shortens the T_2 and T_2* of protons diffusing through the associated magnetic field perturbation. Brain activity, through a poorly understood (4) though long postulated (5) mechanism, triggers local changes in cerebral hemodynamics. Because average increases in blood flow typically outpace apparent changes in local oxygen consumption (6), blood oxygenation increases with neuronal activation. This yields an increase in fMRI signal because the blood becomes less paramagnetic with increasing oxygenation (7, 8). However, opposing this decrease in magnetic field inhomogeneity is an increase in the tissue blood volume (9). It is the balance between changes in blood volume, blood flow and oxygen consumption that dictate the ultimate fMRI contrast.

Several models of fMRI signal change have been proposed. Most have considered primarily the contribution by EV protons (2, 3, 10, 11) using Monte Carlo techniques. EV fMRI models (3, 10), based on typical activation-induced physiological perturbations (2, 3) summarized below, have generally underestimated the gradient echo (GE) signal changes typically observed at 1.5 T, and therefore have inadequately described fMRI signal changes. One potential source of the signal change not accounted for by the EV model are the spins within the vascular space. The IV contribution from a pure phase shift argument was proposed by Haacke *et al.* (12), and the analytical model of Yablonskiy and Haacke (13), valid only in the static dephasing regime, recently considered IV and EV effects in the absence of the oxygenation dependence of the blood's T_2.

The overall goal of this work was to establish the relative contribution of the IV and EV compartments to fMRI signal change. To accomplish this, we extended our EV Monte Carlo model to include the contribution to fMRI signal change from the IV spins. We considered the combined effect of vessel orientation, compartmentalization of the red blood cell (RBC) and the oxygenation dependence of the blood's T_2 on IV signal attenuation at 1.5 T. In the absence of IV compartments, the $3\cos^2\theta-1$ orientation dependence of the IV field shift (14) leads to intravoxel dephasing due to multiple vessel orientations. Vessel size-dependent compartmentalization of red blood cells and the oxygenation dependence of the blood's T_2 (8, 15) enhance the orientation-dependent effects. We then compared our model results with asymmetric spin echo (ASE) data acquired at 1.5 T with and without bipolar gradients to null the IV signal (16–19).

MRM 34:4–10 (1995)

From the NMR Center, Massachusetts General Hospital, Department of Radiology, and Harvard Medical School, Cambridge, Massachusetts (J.L.B., P.A.B., K.K.K., J.R.B., T.L.D., B.R.R., R.M.W.); and Harvard-MIT Division of Health Sciences and Technology, Charlestown, Massachusetts (J.L.B., J.R.B., T.L.D., B.R.R., R.M.W.).

Address correspondence to: Jerrold L. Boxerman, Ph.D., MGH NMR Center, Building 149 (2301), 13th Street, Charlestown, MA 02129.

Received December 8, 1994; revised March 3, 1995; accepted March 27, 1995.

This work was supported in part by NIH grants P01 #48729, R01-HL39810, the Whitaker Foundation and a Clement Vaturi Fellowship.

Results presented in this paper were presented at the 1994 SMR Meeting in San Francisco.

0740-3194/95 $3.00

METHODS

Tissue Model

In our model, fMRI signal may be obtained from both EV and IV spins, and the phase of each spin is influenced by the susceptibility-induced magnetic field changes from both capillaries (radius R_c = 3 μm; volume fraction f_c) and macrovessels (radius R_v; volume fraction f_v), with $f = f_c + f_v$. Signal changes localized to activated cortex (i.e., associated with microvessels) are attributed to spins adjacent to capillaries and to IV capillary spins. Similarly, spins around and within larger venous draining veins may show signal changes, but may be less localized to the site of activation.

To model the noncapillary contribution to EV signal, we used R_v = 25 μm (corresponding to small venules), although quantitatively similar behavior is expected for models with larger R_v (10). For the noncapillary IV contribution, we also considered $R_v \to \infty$ (a large draining vein). We assumed equal volume for capillaries and macrovessels based upon measured capillary (≈2% (20)) and total (≈4% (21)) volume fraction in cortical gray matter. We also assumed that there is slow proton exchange between the EV and IV space (22), and added appropriately weighted signal contributions from the EV and IV compartments to estimate fMRI signal.

Extravascular Signal Attenuation

$\Delta(1/T_2)$ and $\Delta(1/T_2{}^*)$ are linear with respect to recruitment-based changes in f, and quite linear for dilation-based changes for values of f and oxygenation applicable to BOLD experiments. We therefore estimated the EV signal attenuation with respect to fully oxygenated blood at volume fractions exceeding 4% by multiplying properly exponentiated, independent Monte Carlo estimates of EV signal attenuation (3) due to capillaries and venules at a baseline volume fraction of 2% (10).

Blood Signal Attenuation

Using Monte Carlo techniques, we estimated the signal attenuation due to blood (S_b) by simulating the diffusion of protons amidst RBCs within a blood vessel. We modeled the blood as an impenetrable cylindrical compartment with radius R filled at a desired hematocrit (Hct) with fully penetrable spheres (23), representing red blood cells with R = 3 μm and a susceptibility difference with the plasma. The orientation of the cylinder was randomized (with an angular dependence of sin θ) to simulate uniform spatial distribution of vessel orientations within the tissue.

The effect of oxygenation on the T_2 of blood is predominantly due to the dephasing of protons as they diffuse through gradients in and around red blood cells (8). We therefore compared our model ($R \to \infty$, Hct = 40) with *in vitro* T_2 versus hemoglobin oxygenation data obtained at 1.5 T by Wright *et al.* (15) using a modified CPMG sequence with τ_{180} = 24 ms and TE = 72 ms, and fit to a simplified Luz-Meiboom model:

$$1/T_2 \approx 1/T_{2o} + K \cdot (1 - Y)^2 , \qquad [1]$$

with $K = 41.5\ \mathrm{s}^{-1}$, T_{2o} = 249 ms and Y representing the blood oxygenation. Although spheres oversimplify the geometry of erythrocytes, we varied the diffusion coefficient, D, to match the *in vitro* data and used this D value for subsequent simulations. In this manner, the O_2-dependence of T_2 was automatically combined with the orientation and vessel size-dependent geometry effects. We computed IV signal attenuation (with respect to fully oxygenated blood) for capillaries and macrovessels at the "matching" D value as a function of oxygenation. For our simulations, we obtained the susceptibility difference, $\Delta\chi$, between RBC and plasma for a given oxygenation by computing (24):

$$\Delta\chi = \Delta\chi_o \cdot (1 - Y) , \qquad [2]$$

where $\Delta\chi_o = 1.8 \times 10^{-7}$ (cgs units) is the susceptibility between fully deoxygenated whole blood and tissue (24).

Combined Model for fMRI Signal

We assumed that fMRI signal changes are exclusively accounted for by changes in transverse relaxation (e.g., long TR, long TE, echo planar acquisitions), and expressed the prestimulation and poststimulation GE signal, S, in terms of appropriately weighted IV and EV components:

$$S \sim |e^{-TE/T_{2t}^*} A_t + e^{-TE/T_{2b}^*} A_t (f_c A_c + f_v A_v)| . \qquad [3]$$

A_t, A_c, and A_v are the EV tissue, IV capillary and IV macrovessel signal attenuations (0–1) with respect to fully oxygenated blood, respectively, T_{2t}^* is the $T_2{}^*$ of the tissue, and T_{2b}^* is the $T_2{}^*$ of fully oxygenated blood (A_c and A_v account for the oxygenation-dependent $\Delta(1/T_2)$). In well-shimmed cerebral cortex, we typically measure $T_{2t}^* \approx 60$ ms and T_2 = 80 ms. We assumed that T_{2b}^* = 120 ms based on measurements of T_{2b} = 240 ms by Wright *et al.* (15), and that $1/T_2{}' \approx 1/T_{2t}^* - 1/T_{2t} = 1/240$ ms. In general, A_c and A_v are complex quantities (A_t is predominantly real), and hence the measured "signal" is equal to the absolute value of the sum of the real and imaginary components of the IV and EV terms, each weighted by a volume fraction and T_2 factor. Because the phase of each IV spin is influenced by EV gradients from surrounding vessels in addition to IV gradients, A_c and A_v are scaled by A_t.

fMRI Simulation

We modeled a visual stimulation paradigm by computing S for realistic estimates of activation-induced hemodynamic and oxygenation changes. Our fMRI model assumed zero change in oxygen consumption (6); an increase in blood volume equal to the 0.4 power of the relative flow increase ΔF (assuming that flow and volume changes are related in a way that is comparable to PET measurements of hypercapnia (25)); and an initial venous oxygenation of 60% (26). Using a simple transport model (27), we estimated the average capillary oxygenation, $\bar{Q}_c$, from the venous and arterial oxygenation, Q_v

and Q_a, respectively, and the unidirectional oxygen extraction coefficient, $E = 0.5$ (28):

$$\bar{Q}_c = Q_a - (Q_a - Q_v)\left(\frac{1}{E} + \frac{1}{\ln(1-E)}\right). \qquad [4]$$

Equation [4] was obtained by computing the expected value of an expression for Q_c over a normalized capillary segment (27), and limits to $\frac{1}{2}(Q_a + Q_v)$ and Q_v for $E \to 0$ and $E \to 1$, respectively. Equation [4] is relatively insensitive to typical physiological estimates for $E < 0.8$. We also assumed that capillaries and macrovessels each have a prestimulus volume fraction of 2% (4% total); that capillary Hct = 30 and venous Hct = 40 (26); and that both capillaries and larger vessels contribute equally to vascular volume changes (29). In addition, we used an extravascular diffusion coefficient $D = 10^{-5}$ cm^2/s (30). We computed percent signal change (based on prestimulus and poststimulus values of S in Eq. [3]) as a function of flow increase for ΔF between 1.0 and 2.0, and compared the relative contribution of the capillary, macrovascular and total intravascular components by nulling A_v, A_c, and both A_v and A_c, respectively.

Velocity-Sensitized fMRI

To compare our model with experiment, we acquired a series of echo planar images with increasing degrees of diffusion weighting. For an array of randomly oriented vessels with velocity v, a bipolar, z-directed diffusion gradient profile with G G cm^{-1} gradients, pulse width δ and time between onset of the pulses equal to Δ will provide significant signal attenuation for $kv_t > \pi$, where v_t is a sequence-dependent velocity threshold, and

$$k = 2\pi\gamma \int tG\,dt = 2\pi\gamma G\delta\Delta\,. \qquad [5]$$

Similarly, any large vessel with plasma velocity spread Δv such that $k\Delta v > \pi$ will also suffer significant signal attenuation. The diffusion weighting (b value) for such a sequence is approximately

$$b = (2\pi\gamma G)^2\delta^2\left(\Delta - \frac{\delta}{3}\right). \qquad [6]$$

For each experimental run, we acquired 4 min of visual stimulation data (alternating between 60 s of fixation point only and 60 s of full-field counter-phased checkerboard flickering at 8 Hz) with a diffusion-weighted (bipolar, z-directed, G = 1 G/cm, $\Delta = \delta + 5$ ms) ASE sequence ($\tau = -20$ ms, TE = 165 ms, TR = 2 s) on a Signa 1.5 T scanner (General Electric, Milwaukee, WI) retrofitted for echo planar imaging (Advanced NMR, Wilmington, MA). A TR of 2 s was chosen to reduce the inflow effect of approximately 0.5% reported previously for TR = 1 s (31). The ASE sequence with these parameters provides similar T_2' contrast to a gradient acquisition with TE = 40 ms (32). We acquired data with pulse widths of δ = 0, 10, 20, 30, 40, and 50 ms, which yielded a velocity sensitivity of π radians for $v_t = 1/(2\gamma G\delta\Delta) = \infty$, 0.8, 0.2, 0.1, 0.07, and 0.04 cm/s, respectively, and associated diffusion weightings of $b \approx 0$ (ignoring the small contribution of the imaging gradients), 10, 50, 160, 360, and 690 s mm^{-2}, respectively. The in-plane resolution was 3×3 mm^2 with a slice thickness of 7 mm.

For each of five subjects, we performed a separate visual stimulation experiment for each of the above pulse widths and associated b values and imaged an oblique slice through the visual cortex containing the calcarine fissure. For each b = 0 data set, we computed the temporal cross correlation (33) between the experimental time course in each voxel and the expected temporal response (temporally shifted boxcar function). Those voxels for which the correlation coefficient exceeded 0.5 comprised a ROI from which a spatially averaged time course was obtained for each successive b value. This threshold yielded ROIs (42–45 voxels), which were likely to contain on average the cortical blood volume fractions assumed in our model. We applied a three-point median filter (34) to each time course to remove signal intensity discontinuities due to cardiac pulsations that are typically observed for nongated acquisitions at large b values (35). We then measured the percent signal change for each time course by comparing the initial baseline with the average activation plateau (subsequent baselines were disregarded to eliminate inclusion of any undershoot). Each percent signal change was then compared with the percent signal change obtained in the absence of diffusion (b = 0) to determine a normalized attenuation at each b value.

RESULTS

Blood Signal Attenuation

Figure 1 compares $\Delta(1/T_2 = -\ln(S)/TE$ from the Monte Carlo blood model ($D = 10^{-5}$ cm^2/s) for an infinite pool of red blood cells and for R = 25 μm cylinders with the *in vitro* experimental data of Wright *et al.* (15) (Eq. [1],

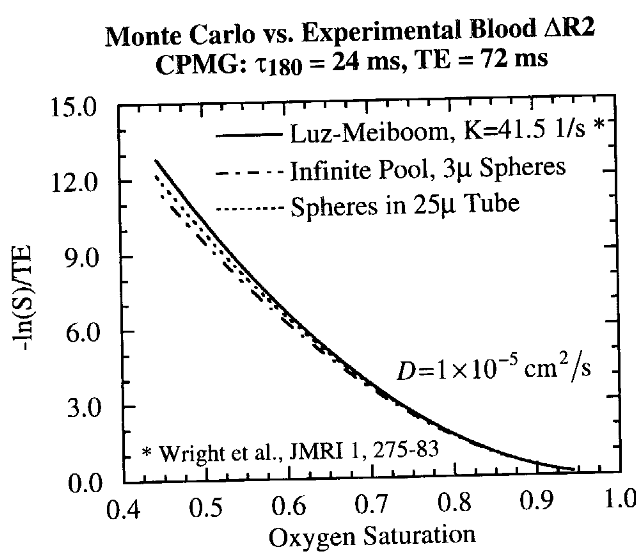

FIG. 1. Monte Carlo versus experimental ΔR2 in blood (simulated Hct = 40) using a CPMG sequence, with τ_{180} = 24 ms and TE = 72 ms. Simulation matches experiment for $D = 10^{-5}$ cm^2/s. The Luz-Meiboom K value was obtained from the experimental data of Wright *et al.* (15).

with $K = 41.5\ \mathrm{s}^{-1}$ and $T_{2o} = 249$ ms). The predicted T_2 dependence on blood oxygenation agrees well with experiment at this D value, suggesting that our simplified corpuscular blood model accounts for the predominant T_2 effects in large vessels.

Figure 2 plots extravascular GE signal attenuation at 1.5 T due to capillaries ($f_c = 2\%$; Hct = 30) and venules ($f_v = 2\%$; Hct = 40) as a function of oxygenation for $TE = 40$ ms. Also plotted are the real and imaginary components of intravascular GE signal attenuation due to capillaries and venules as a function of oxygenation. Figure 2 demonstrates that the EV signal attenuation has no phase shift, and that the IV signal attenuation has relatively minor phase shift at 1.5 T. Whereas relatively small signal attenuations are predicted due to the EV spins for typical oxygenation changes, substantially greater signal attenuation is realized from the intravascular spins within both capillaries and venules.

fMRI Simulation

Figure 3 compares predicted signal change for GE acquisitions with $TE = 40$ ms at 1.5 T with no IV effects ($A_c = 0$ and $A_v = 0$ in Eq. [3]), and with IV effects due to capillaries ($A_v = 0$), macrovessels ($A_c = 0$; $R_v = 25\ \mu$m), and both capillaries and macrovessels. Quantitatively similar results were obtained for the IV macrovessel model with $R_v \rightarrow \infty$. For typical 60–80% flow increases (shaded region), the model suggests that the blood itself contributes significantly and accounts for approximately two-thirds of the total GE signal change. The model predicts total and EV signal changes of ≈3% and 1%, respectively at $TE = 40$ ms. The isolated contribution of the macrovessels exceeds that of the capillaries.

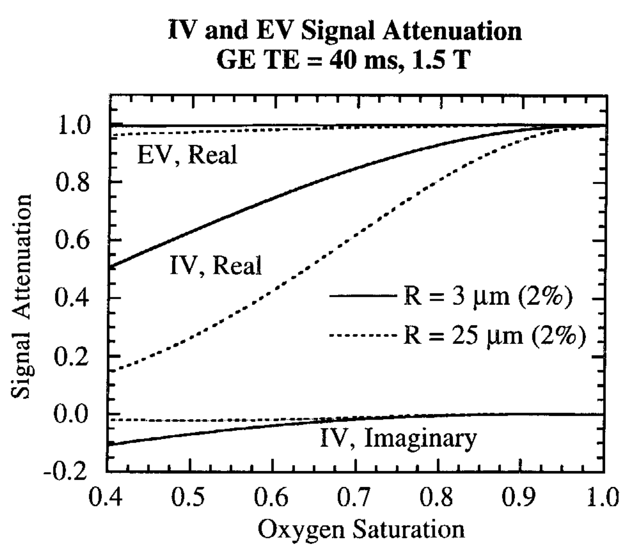

FIG. 2. Extravascular and intravascular GE signal attenuation at 1.5 T due to capillaries ($f_c = 2\%$; Hct = 30) and venules ($f_v = 2\%$; Hct = 40) as a function of oxygenation for $TE = 40$ ms. The EV signal attenuation has no phase shift, and the IV signal attenuation has relatively minor phase shift at 1.5 T. Whereas relatively small EV signal attenuations are predicted for typical oxygenation changes, substantially greater signal attenuation is realized from the intravascular spins.

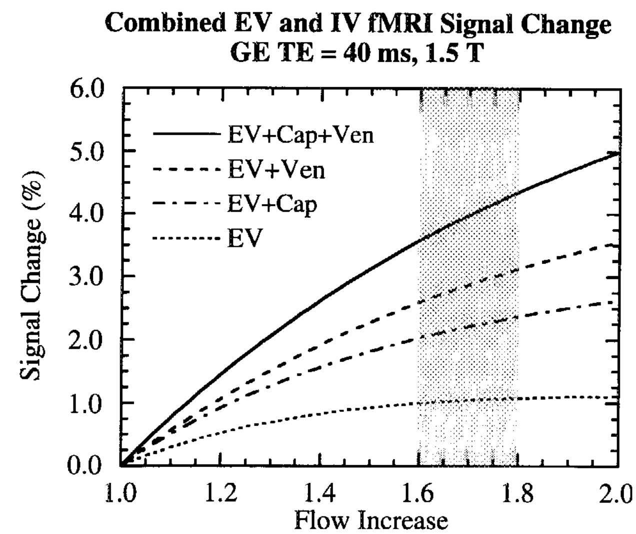

FIG. 3. A comparison of the predicted GE ($TE = 40$ ms) fMRI signal change at 1.5 T with no IV effects (EV), IV effects due solely to capillaries (EV + Cap), IV effects due solely to venous vessels (EV + Ven; $R_v = 25\ \mu$m), and IV effects due to both capillaries and venules (EV + IV). Quantitatively similar results were obtained for the IV macrovessel model with $R_v \rightarrow \infty$. For typical 60–80% flow increases (shaded region), the model predicts total and EV signal changes of ≈3% and 1%, respectively, suggesting that the blood itself accounts for approximately two-thirds of the total GE signal change. The isolated contribution of venules exceeds that of capillaries.

Velocity-Sensitized fMRI

Figure 4 shows the correlation coefficient maps from one of the subjects in this study at b values of 0, 10, 50, and 160 s mm^{-2}. Although the degree of activation decreases with increasing b value, the spatial pattern of activation

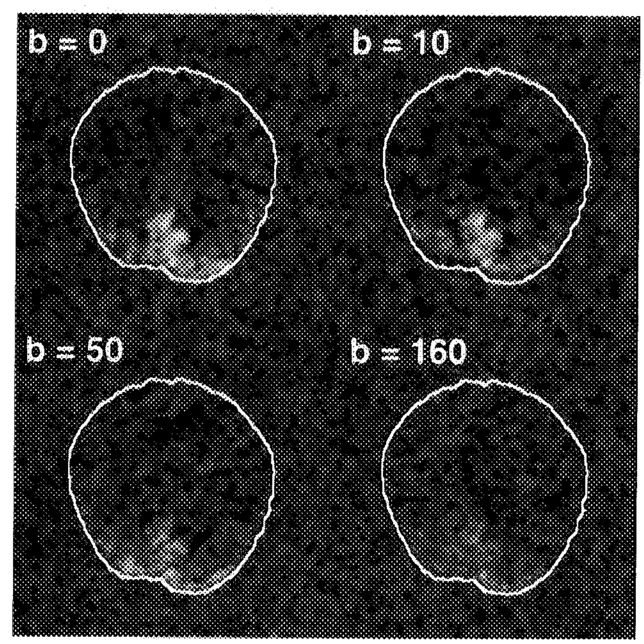

FIG. 4. The correlation coefficient maps from a typical subject at b values of 0, 10, 50, and 160 s mm^{-2}. Although the degree of activation decreases with increasing b value, the spatial extent of the activation does not change dramatically.

is preserved. Figure 5 illustrates the effect of diffusion weighting on fMRI signal for a typical velocity-sensitized ASE fMRI experiment at 1.5 T with TE = 165 ms and τ = −20 ms. Median-filtered data are plotted for acquisitions with b = 0, 10, 50, and 160 s mm^{-2}, and the corresponding percent signal changes of 2.9, 1.5, 1.8, and 1.6% were computed based on the average baseline and activation plateaus as indicated in the figure. The median filter removes many of the spikes that occur at high b values while preserving the overall structure of the time course. The attenuations with respect to the b = 0 acquisition from five subjects were averaged and plotted as a function of b in Fig. 6. A b value as small as 10 s mm^{-2} attenuated the percent signal change by approximately 30%. As b is increased, the attenuation increases, and ultimately reaches a plateau at approximately 70% attenuation.

DISCUSSION

In this work, we presented a Monte Carlo model for BOLD signal change that is unique in its inclusion of *both* the intravascular and extravascular contribution to gradient echo signal change. Our simulations suggest that the intravascular spins account for the majority of fMRI signal change at 1.5 T, even in regions where the vascular volume fractions are small (4–6%). We compared our model results with experimental fMRI signal changes obtained with and without velocity sensitization via bipolar gradients to null the contribution of intravascular, rapidly flowing spins. With increasing diffusion weighting, the activation-induced signal change decreased from 3% at b = 0 and appeared to plateau at roughly 1% for b values exceeding 360 s mm^{-2}. These signal changes agree with those predicted by our model. The large b values that we used should be sufficient to eliminate the intravascular contribution from spins within vessels of all sizes, including capillaries. During the velocity-sensitized period of 100 ms used to generate b = 690 s mm^{-2}, a spin traveling at the average capillary corpuscular velocity of 0.2 cm/s (20) will traverse a distance of 200 μm, which exceeds the typical capillary segment length of ≈ 100 μm (20), and should therefore experience velocity-related attenuation. Furthermore, the corresponding velocity threshold of 0.04 cm/s is well below the average capillary RBC velocity. Therefore, the results of both the model and the experiment strongly suggest that the intravascular spins account for the majority, though not the totality, of T_2^*-weighted fMRI signal change at 1.5 T.

The model also predicts that the intravascular contribution of venules and veins exceeds that of capillaries, despite similar volume fractions. There are two explanations for this. First, assuming minimal dilution, the oxygenation of the venous blood after traversing the capillary bed is substantially less than the average capillary blood oxygenation, as seen in Eq. [4]. Second, for equivalent oxygenation, spins within venular-sized or larger vessels produce greater changes in T_2* than spins within capillaries, as demonstrated in Fig. 2. However, the capillary contribution is significant, as predicted in Fig. 3, which suggests that we can null the macrovascular IV effect and still retain substantial fMRI signal. These results are supported by the experiment, which demonstrates increasing attenuation of activation-induced signal change with b, and large attenuation even for very small b values corresponding to velocity thresholds exceeding 0.8 cm/s. The activation-induced signal change was reduced by about 30% at b = 10 s mm^{-2}. Based on known plasma flow rates, only the signal from veins and some fraction of venules should be nulled at this b value. Increasing the b value from 10 to 690 s mm^{-2} roughly doubles the attenuation, though does not eliminate it. If the IV macrovascular contribution were insignificant, we would be less motivated to eliminate it, because IV capillary and venular contributions are likely to be localized, at least within 1.5 mm, to the site of activation (36).

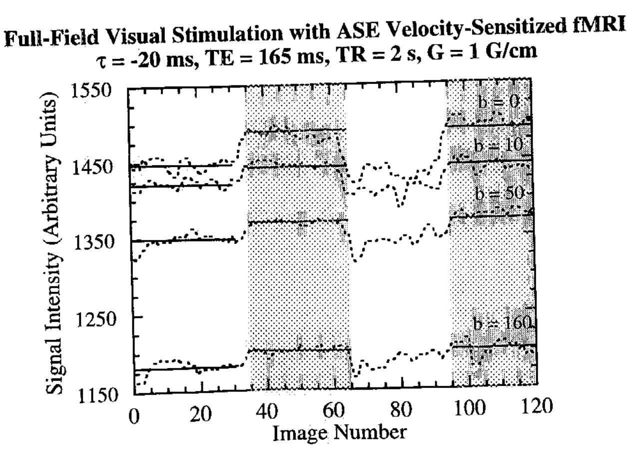

FIG. 5. Results from a typical velocity-sensitized ASE fMRI experiment at 1.5 T with TE = 165 ms and τ = −20 ms. Median-filtered data (dashed lines) are plotted for acquisitions with b = 0, 10, 50, and 160 s mm^{-2}, and the corresponding percent signal changes of 2.9, 1.5, 1.8, and 1.6% were computed based on the average baseline and activation plateaus (solid lines).

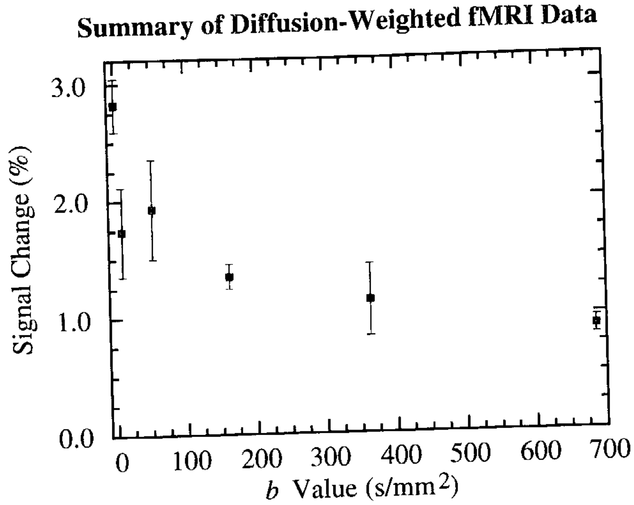

FIG. 6. The average (n = 5) percent signal change plotted as a function of b. At a b value as small as 10 s mm^{-2}, the percent signal change is attenuated by approximately 30%. Increasing the b value from 10 to 690 s mm^{-2} roughly doubles the attenuation, which ultimately plateaus at approximately 70% attenuation.

Our model utilizes a variety of assumptions about the fundamental physiology, including volume fraction distribution between capillaries and venules, and the initial volume fraction and oxygenation. However, using literature values for these parameters, the model satisfactorily predicts both the absolute and relative contribution due to the extravascular and intravascular spins in the visual stimulation paradigm. Our model applies to homogeneous cortex with no partial volume effects of very large vessels that could account for significantly larger (>10%) volume fractions of draining veins or sinuses. We believe that the large ROIs chosen for our experimental data reflect this condition on average. The correlation images depicted in Fig. 4 demonstrate that the activation decreases with increasing b value. However, even with increased b, the spatial extent of the activation-induced signal does not change dramatically. This suggests that the decrease in the spatially-averaged activation-induced signal does not likely come from removing the contribution of a few isolated veins, but is more likely due to reduced intravoxel, intravascular contributions. As the imaging resolution increases, our homogeneous tissue model becomes less valid. Using high-resolution fMRI acquisitions, Frahm *et al.* (37) and Lai *et al.* (38) documented very large signal changes for voxels with substantial blood volume fractions. Our model is not scale invariant, and is less applicable to such inhomogeneous volume distributions. Our results should be interpreted for typical imaging resolutions employed by our group and others at 1.5 T.

We conclude from our model and experimental results that the intravascular spins account for the majority of T_2*-weighted fMRI signal change in true cortex at 1.5 T, even for an average tissue volume fraction of only 4–6%. An important question arising from the study of intravascular contrast is how we might minimize the contribution from larger vessels which may not be localized to the site of activation. Diffusion-weighted sequences with modest b values appear capable of attenuating signal from larger blood vessels. These results suggest that velocity-sensitized fMRI may have potential for reducing or eliminating the large vessel intravascular contribution (putatively less well-localized to neuronal activity) with judicious choice of diffusion weighting, and for enhancing the spatial selectivity of fMRI. However, in T_2*-weighted sequences, the extravascular contribution from macrovessels remains even in the presence of velocity sensitization. Nevertheless, the model presented here and its comparison to velocity-sensitized ASE imaging provides a new handle on quantifying fMRI signal changes and relating these changes to the underlying neuronal activity.

REFERENCES

1. S. Ogawa, T. Lee, A. Kay, D. Tank, Brain magnetic resonance imaging with contrast dependent on blood oxygenation. *Proc. Natl. Acad. Sci. (USA)* **87,** 9868–9872 (1990).
2. S. Ogawa, R. Menon, D. Tank, S. Kim, H. Merkle, J. Ellermann, K. Ugurbil, Functional brain mapping by blood oxygenation level-dependent contrast magnetic resonance imaging: a comparison of signal characteristics with a biophysical model. *Biophys. J.* **64,** 803–812 (1993).
3. R. Weisskoff, J. Boxerman, C. Zuo, B. Rosen, *in* "Functional MRI of the Brain, SMRM Workshop, Arlington, VA, 1993," pp. 103–110.
4. H. Lou, L. Edvinsson, E. MacKenzie, The concept of coupling blood flow to brain function: revision required? *Ann. Neurol.* **22,** 289–297 (1987).
5. C. Roy, C. Sherrington, On the regulation of the blood-supply of the brain. *J. Physiol. (Lond.)* **11,** 85–108 (1890).
6. P. Fox, M. Raichle, Focal physiological uncoupling of cerebral blood flow and oxidative metabolism during somatosensory stimulation in human subjects. *Proc. Natl. Acad. Sci. (USA)* **83,** 1140–1144 (1986).
7. L. Pauling, C. Coryell, The magnetic properties and structure of hemoglobin, oxyhemoglobin and carbon monooxyhemoglobin. *Proc. Natl. Acad. Sci. (USA)* **22,** 210–216 (1936).
8. K. Thulborn, J. Waterton, P. Matthews, G. Radda, Oxygenation dependence of the transverse relaxation time of water protons in whole blood at high field. *Biochem. Biophys. Acta.* **714,** 265–270 (1982).
9. J. Belliveau, D. Kennedy, R. McKinstry, B. Buchbinder, R. Weisskoff, M. Cohen, J. Vevea, T. Brady, B. Rosen, Functional mapping of the human visual cortex using magnetic resonance imaging. *Science* **254,** 716–719 (1991).
10. J. Boxerman, R. Weisskoff, B. Hoppel, L. Hamberg, B. Rosen, *in* "Proc., SMRM, 12th Annual Meeting, New York, 1993," p. 389.
11. R. Kennan, J. Zhong, J. Gore, Intravascular susceptibility contrast mechanisms in tissues. *Magn. Reson. Med.* **31,** 9–21 (1994).
12. E. Haacke, A. Hopkins, S. Lai, P. Buckley, L. Friedman, H. Meltzer, P. Hedera, R. Friedland, S. Klein, L. Thompson, D. Detterman, J. Tkach, J. Lewin, 2D and 3D high resolution gradient echo functional imaging of the brain: Venous contributions to signal in motor cortex studies. *NMR Biomed.* **7,** 54–62 (1994).
13. D. Yablonskiy, E. Haacke, Theory of NMR signal behavior in magnetically inhomogeneous tissues: The static dephasing regime. *Magn. Reson. Med.* **32,** 749–763 (1994).
14. S. Chu, Y. Xu, J. Balschi, C. Springer, Bulk magnetic susceptibility shifts in NMR studies of compartmentalized samples: Use of paramagnetic reagents. *Magn. Reson. Med.* **13,** 239–262 (1990).
15. G. Wright, B. Hu, A. Macovski, Estimating Oxygen Saturation of Blood in Vivo with MR Imaging at 1.5 T. *J. Magn. Reson. Imaging,* **1,** 275–283 (1992).
16. J. Boxerman, R. Weisskoff, K. Kwong, T. Davis, B. Rosen, *in* "Proc., SMR, 2nd Annual Meeting, San Francisco, 1994," p. 619.
17. K. Kwong, D. Chesler, J. Boxerman, T. Davis, R. Weisskoff, B. Rosen, *in* "Proc., SMR, 2nd Annual Meeting, San Francisco, 1994," p. 650.
18. A. Song, E. Wong, P. Bandettini, J. Hyde, *in* "Proc., SMR, 2nd Annual Meeting, San Francisco, 1994," p. 643.
19. R. Menon, X. Hu, G. Adriany, P. Andersen, S. Ogawa, K. Ugurbil, *in* "Proc., SMR, 2nd Annual Meeting, San Francisco, 1994," p. 622.
20. G. Pawlik, A. Rackl, R. Bing, Quantitative capillary topography and blood flow in the cerebral cortex of cats: An *in vivo* microscopic study. *Brain Res.* **208,** 35–58 (1981).
21. K. Leenders, D. Perani, A. Lammertsma, J. Heather, P. Buckingham, M. Healy, J. Gibbs, R. Wise, J. Hatazawa, S. Herold, R. Beaney, D. Brooks, T. Spinks, C. Rhodes, R. Frackowiak, T. Jones, Cerebral blood flow, blood volume and oxygen utilization: normal values and effect of age. *Brain* **113,** 27–47 (1990).
22. O. Paulson, M. Hertz, T. Bolwig, N. Lassen, Filtration and diffusion of water across the blood-brain barrier in man.

Microvasc. Res. **13,** 113–124 (1977).
23. M. Herbst, J. Goldstein, A review of water diffusion measurement by NMR in human red blood cells. *Am. J. Physiol.* **256,** C1097–C1104 (1989).
24. R. Weisskoff, S. Kiihne, MRI susceptometry: image-based measurement of absolute susceptibility of MR contrast agents and human blood. *Magn. Reson. Med.* **24,** 375–383 (1992).
25. R. Grubb, M. Raichle, J. Eichling, M. Ter-Pogossian, The effects of changes in PaCO2 on cerebral blood volume, blood flow, and vascular mean transit time. *Stroke* **5,** 630–639 (1974).
26. A. Guyton, "Textbook of Medical Physiology," W.B. Saunders Co., Philadelphia, 1991.
27. H. Larsson, M. Stubgaard, J. Frederiksen, M. Jensen, O. Henriksen, O. Paulson, Quantitation of blood-brain barrier defect by magnetic resonance imaging and gadolinium-DTPA in patients with multiple sclerosis and brain tumors. *Magn. Reson. Med.* **16,** 117–131 (1990).
28. N. Alpert, R. Buxton, J. Correia, P. Katz, R. Ackerman, Measurement of end-capillary pO2 with positron emission tomography. *J. Cereb. Blood Flow Metab.* **8,** 403–410 (1988).
29. R. Duelli, W. Kuschinsky, Changes in brain capillary diameter during hypocapnia and hypercapnia. *J. Cereb. Blood Flow Metab.* **13,** 1025–1028 (1993).
30. A. Bizzi, A. Righini, R. Turner, D. LeBihan, D. DesPres, G. Di Chiro, J. Alger, MR of diffusion slowing in global cerebral ischemia. *Am. J. Neuroradiol.* **14,** 1347–1354 (1993).
31. P. Bandettini, E. Wong, R. Cox, A. Jesmanowicz, R. Hinks, J. Hyde, *in* "Proc., SMR, 2nd Annual Meeting, San Francisco, 1994," p. 621.
32. J. Baker, B. Hoppel, C. Stern, K. Kwong, R. Weisskoff, B. Rosen, *in* "Proc., SMRM, 12th Annual Meeting, New York, 1993," p. 1400.
33. P. Bandettini, A. Jesmanowicz, E. Wong, J. Hyde, Processing strategies for time-course data sets in functional MRI of the human brain. *Magn. Reson. Med.* **30,** 161–173 (1993).
34. J. Lim, "Two-Dimensional Signal and Image Processing," Prentice Hall, Englewood Cliffs, NJ, 1990.
35. R. McKinstry, R. Weisskoff, J. Belliveau, J. Vevea, J. Moore, K. Kwong, E. Halpern, B. Rosen, Ultrafast MR imaging of water mobility: Animals of altered cerebral perfusion. *J. Magn. Reson. Imaging* **2,** 337–384 (1992).
36. H. Duvernoy, S. Delon, J. Vannson, Cortical blood vessels of the human brain. *Brain Res. Bull.* **7,** 519–579 (1981).
37. J. Frahm, K. Merboldt, W. Hänicke, Functional MRI of human brain activation at high spatial resolution. *Magn. Reson. Med.* **29,** 139–144 (1993).
38. S. Lai, A. Hopkins, E. Haacke, D. Li, B. Wasserman, P. Buckley, L. Friedman, H. Meltzer, P. Hedera, R. Friedland, Identification of vascular structures as a major source of signal contrast in high resolution 2D and 3D functional activation imaging of the motor cortex at 1.5 T: Preliminary results. *Magn. Reson. Med.* **30,** 387–392 (1993).